ELSEVIER

Journal of Fluids and Structures 24 (2008) 270–280

JOURNAL OF FLUIDS AND STRUCTURES

www.elsevier.com/locate/jfs

Fluid–solid interaction simulation of flow and stress pattern in thoracoabdominal aneurysms: A patient-specific study

A. Borghi[a,*], N.B. Wood[a], R.H. Mohiaddin[b], X.Y. Xu[a]

[a]*Department of Chemical Engineering, South Kensington Campus, Imperial College, London SW72AZ, UK*
[b]*Royal Brompton and Harefield NHS Trust, Sydney Street, London, UK*

Received 2 December 2006; accepted 18 August 2007
Available online 19 November 2007

Abstract

Thoracoabdominal aneurysm (TA) is a pathology that involves the enlargement of the aortic diameter in the inferior descending thoracic aorta and has risk factors including aortic dissection, aortitis or connective tissue disorders. Abnormal flow patterns and haemodynamic stress on the diseased aortic wall are thought to play an important role in the development of this pathology and the internal wall stress has proved to be more reliable as a predictor of rupture than the maximum diameter for abdominal aortic aneurysms; but this assumption has not been validated yet for aneurysms involving the thoracic aorta. In the present study, three patients with TAs of different maximum diameters were scanned using magnetic resonance imaging (MRI) techniques. Realistic models of the aneurysms were reconstructed from the *in vivo* MRI data acquired from the patients, and subject-specific flow conditions were applied as boundary conditions. The wall and thrombus were modelled as hyperelastic materials and their properties were derived from the literature. A normal descending aorta was also simulated to provide data for comparison. Fully coupled fluid–solid interaction (FSI) simulations as well as solid static simulations were performed using ADINA 8.2. The results show that the wall stress distribution and its magnitude are strongly dependent on the 3-D shape of the aneurysm and the distribution of thrombus. Maximum wall stresses in all TA models are higher than in the normal aorta, and values of maximum wall stress are not directly related to the maximum aneurysm diameter. Comparisons between the FSI and solid static simulation results showed no significant difference in maximum wall stress, supporting those previous studies which found that FSI simulations were not necessary for wall stress prediction.

Keywords: Thoracoabdominal aneurysm; Magnetic resonance imaging; Fluid–solid interaction; Intra-luminal thrombus

1. Introduction

An aneurysm is an abnormal localized enlargement of a portion of an artery, related to weakness in the wall of the blood vessel. The associated mortality rate is particularly high: thoracoabdominal aneurysms (TAs) reaching the size of 6–10 cm or above tend to rupture or dissect in 62% of the cases (Webb and Williams, 1999) and surgical interventions are usually recommended for aneurysms 0.5 cm below the critical diameter (Elefteriades, 2002). However, surgical

*Corresponding author. Tel.: +442075945588
E-mail addresses: alessandro.borghi@imperial.ac.uk (A. Borghi), n.wood@imperial.ac.uk (N.B. Wood), r.mohiaddin@rbht.nhs.uk (R.H. Mohiaddin), yun.xu@imperial.ac.uk (X.Y. Xu).

0889-9746/$ - see front matter © 2007 Elsevier Ltd. All rights reserved.
doi:10.1016/j.jfluidstructs.2007.08.005

repairs of TA are not without risks and the costs are relatively high: operating on patients with ruptured or dissected aneurysms involves mortality in 15% of the cases or more (Culliford et al., 1983); furthermore, surgical repair of aneurysms has serious drawbacks, such as paraparesis or paraplegia in 4.6% of the cases (LeMaire et al., 2003). Moreover, a recent study has suggested that the failure of ascending thoracic aneurysm wall is not related to its diameter (Vorp et al., 2003).

Previous studies, focused mainly on abdominal aortic aneurysms (AAAs), suggested that the peak wall stress was a more reliable parameter for the assessment of the rupture risk in these cases. Fillinger et al. (2003) reported that the peak wall stress in aneurysms had a higher sensitivity and specificity for predicting the rupture than maximum diameter (94%, 81% versus 81%, 70%). Venkatasubramaniam et al. (2004) analysed 27 AAAs using finite element techniques, of which 15 had ruptured after the scan. The wall stress was found to be significantly higher in the ruptured aneurysms and the rupture site coincided with the area of maximum wall stress. On the other hand, abnormal flow patterns and recirculation were found to occur in AAAs. Bluestein et al. (1996) investigated the role of disturbed flow on platelet deposition and thrombus formation in an aneurysm model using numerical as well as experimental methods, and showed that platelets with elevated shear histories and higher incidence of activation tended to adhere to the wall in areas of low wall shear stress (WSS). The effect of dynamic interactions between blood flow and wall motion in AAAs has been investigated and the first such work was performed by Di Martino et al. (2001), who analysed the complex stress pattern and fluid dynamics in a patient-specific aneurysm model. Later studies evaluated the importance of coupled fluid structure interaction (FSI) for calculating the stress pattern in patient-specific aneurysm models. In this respect, different opinions are present in the literature: Leung et al. (2006) and Wolters et al. (2005) state that little change in stress (around 0.1%) is caused by the presence of flow inside the aneurysm, and that the flow-induced pressure variation is negligible in comparison with the pulse pressure applied in the aneurysm model. Scotti et al. (2005) instead point out that static solid models may underestimate the stress by 10–30%, especially if the aneurysm is modelled using variable wall thickness; Papaharilaou et al. (2006) draw similar conclusions using a decoupled approach, showing that isolated static structural stress analysis captures the main features of the stress distribution but underestimates the magnitude of the peak wall stress by approximately 12%.

Although a significant amount of work has been carried out on the role of mechanical stress in the development of aneurysms in the abdominal aorta, little has been done on aneurysms involving the descending thoracic aorta, where, even in normal subjects, a complex flow pattern may exist (Wood et al., 2001). In the present work, three TAs were reconstructed from *in vivo* MR images and the stress and velocity patterns simulated using patient-specific flow conditions. The results show how the stress pattern and values are influenced by the shape of the aneurysm and the presence of intra-luminal thrombus (ILT). A normal descending aorta was also simulated to provide data for comparison.

2. Methods

The TA models of three patients were reconstructed from MRI data. Multiple high-resolution 2-D HASTE (half-Fourier acquisition single-shot turbo spin-echo) images were acquired to assess the site, shape and wall of the aortic aneurysm. According to the Crawford classification of TA (Crawford et al., 1986), all patients have type I TAs (the aneurysm originates below the subclavian artery and involves most of the descending thoracic aorta). The maximum aneurysm diameters, measured as the maximum cross-sectional dimension extracted from the scans, were 7.0, 6.2 and 7.0 cm for patients A, B and C, respectively. Table 1 summarizes the MR scan parameters used in this study.

A semi-automatic image segmentation programme implemented via MATLAB was used to delineate the internal and external surface contours of the aneurysms from the HASTE images. This programme has been validated previously using carotid phantoms with known geometry (Augst et al., 2003; Cheong, 2004), An initial step of median filtering (a type of low-pass Gaussian filter) was applied to reduce the noise in the images. Since the procedure involved manual segmentation which was performed by the same operator for all subjects examined, the reproducibility of intra-operator segmentation was assessed. This was performed on patient B by comparing lumen and wall contours extracted by the same operator at three different times. A maximum mean difference of 4.6% in area between results obtained from two different attempts was found.

The results of the segmentation are shown in Fig. 1, where the arrows indicate the locations of ILT. Patient A has ILT at one site only while Patient B has developed ILT at two locations. Patient C has a similar morphology to that of patient A, showing a large thrombus formation on one side of the aortic wall. Mural thrombus is a common feature in aortic aneurysms: Machida and Tasaka (1980) found that in a population of 71 patients with aneurysms, of which 33 with thoracic aneurysm, 25 with abdominal and 13 with TA, ILT was visible in CT in 86% of the cases.

Table 1
Summary of the parameters used for the MR scans

	Patient A		Patient B		Patient C	Control case
	Set A1	Set A2	Set B1	Set B2	Set C	Set D
	HASTE[a]	PC Vel mapping[a]	HASTE	PC Vel mapping[a]	HASTE[a]	HASTE[a]
Slice thickness (mm)	6	8	6	8	6	6
Number of images	20	20	25	20	40	25
TR (ms)	800	58	660	55	590	700
TE (ms)	23	3.1	23	2.8	42	42

[a]Image type.

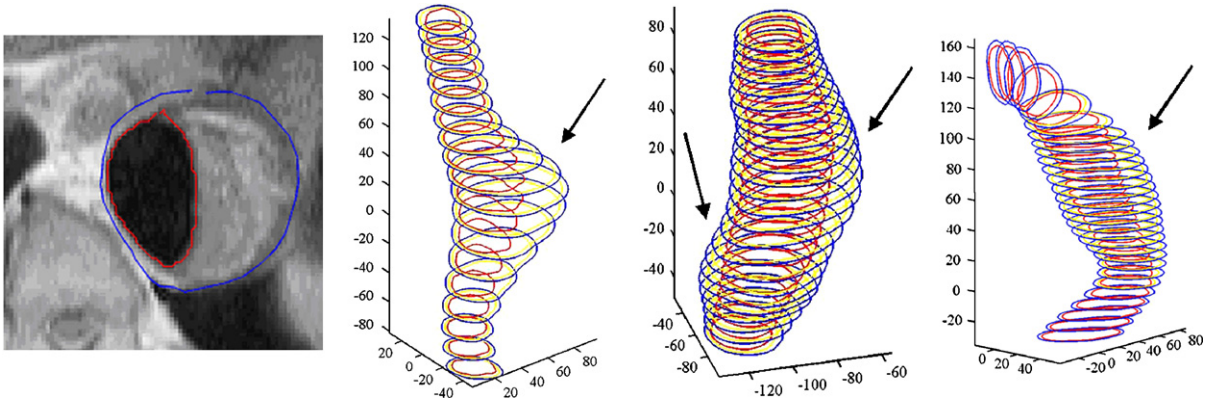

Fig. 1. Example of the segmentation of patient A (left) and reconstructed models for patients A, B and C (units in mm); the arrows show the locations of ILT.

A set of 3-D smoothing procedures (using least squares cubic splines) was developed for performing contour smoothing and surface smoothing, similar to methods previously used in our group (Long et al., 2000). This step was performed in order to remove possible registration errors and refine the final geometry to obviate sharp corners that may create spurious stress levels in the final solution (Moore et al., 1999). The wall thickness was determined by taking the average value of 12 measurements made at sections where wall thickness was clearly defined, using an approach similar to that adopted by Wang et al. (2002). The wall thickness was 3.44 ± 0.42 mm for patient A, 3.05 ± 0.35 mm for patient B and 3.08 ± 0.33 for patient C. The inner wall contours were created by shrinking the corresponding outer wall contours uniformly to match the measured wall thickness. Fig. 2 shows an example of the wall thickness measurement.

The flow information for patients A and B was obtained from cine phase-contrast velocity mapping. Patient-specific flow-rates were calculated by performing integration of the velocity profiles at the inlet and these were used as inlet conditions for flow simulations. Fig. 3 shows the volumetric flow rate curves for patients A and B.

Time-dependent pressure was specified at the model outlet: since pressure was not recorded for these patients, a typical pressure waveform for a healthy subject found from the literature was used (Olufsen et al., 2000) (see Fig. 4). In the simulations presented here, pressure differences from the diastolic pressure were specified so the stress values shown should be considered as stress increments from the corresponding values in diastole. A phase shift of 0.1 s (corresponding to a physiological value) between the peak flow and peak pressure was set.

The TA models and the normal aorta were subdivided using tetrahedral elements for the fluid (or lumen) domain and hexahedral elements for the wall domain. The wall was modelled as a homogeneous hyperelastic material with a stress–stretch relationship given by

$$T = [2\alpha + 4\beta(\lambda^2 + 2\lambda^{-1} - 3)](\lambda^2 - \lambda^{-1}),$$

where T is the stress and λ is the stretch ratio. For ascending TA strips, Vorp et al. (2003) found values for the constants as $\alpha = 100$ kPa and $\beta = 530$ kPa. A similar relation was assumed for the thrombus, whose material properties were

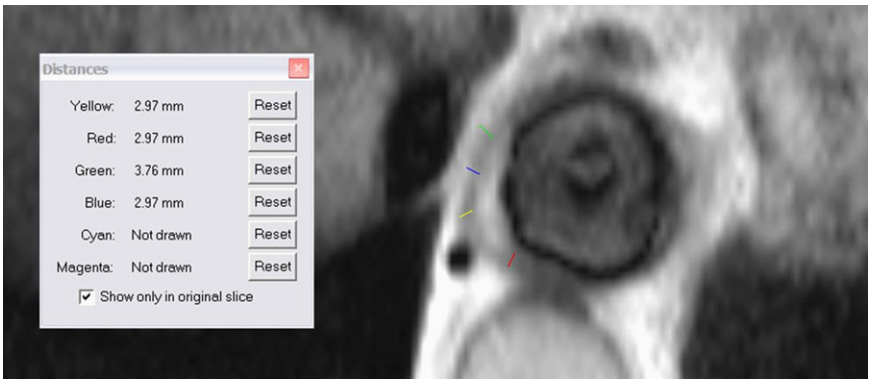

Fig. 2. Example for the wall thickness measurement.

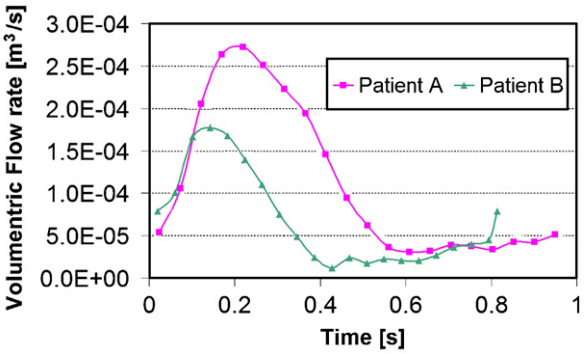

Fig. 3. Flow rate curves for patients A and B.

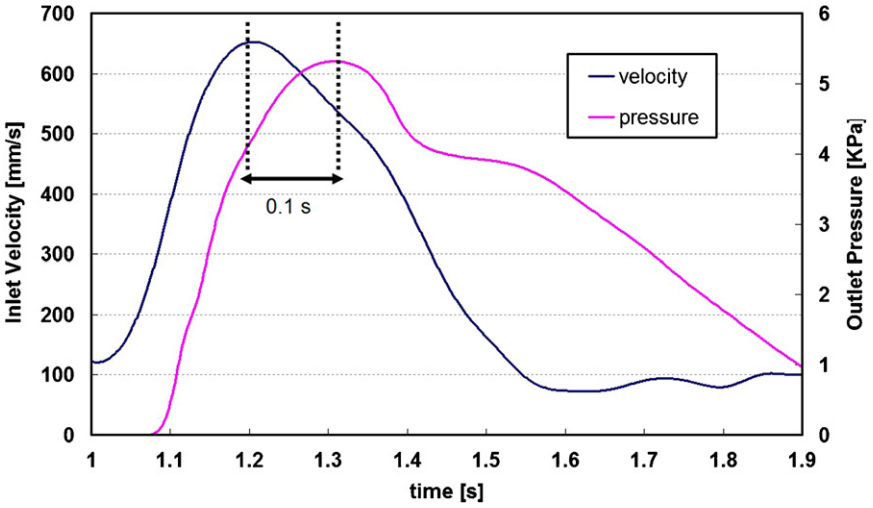

Fig. 4. Pressure waveform applied at the outlet of the FSI models showing assumed phase lag between peak systolic velocity and peak systolic pressure.

retrieved by Wang et al for thrombus in AAAs with values of $\alpha = 28\,\text{kPa}$ and $\beta = 28.6\,\text{kPa}$ (Wang et al., 2001). The blood was assumed to be incompressible and Newtonian, with a constant viscosity $\mu = 4 \times 10^{-3}\,\text{Pa s}$ and density $\rho = 1060\,\text{kg/m}^3$. For the solid domain, both ends were constrained (longitudinally and radially) to simulate the tethering to the rest of the aorta. At the thrombus and wall interface the same number of elements was used and the

displacement was continuous across the two domains. At the two ends of the thrombus a tied interface condition was applied, in order to prevent sliding. This interface condition allows no sliding between the surfaces in contact and can be used to connect surfaces having incompatible meshes. It is based on the segment method algorithm available in ADINA, which uses the Lagrangian multiplier to enforce the contact condition and has been shown to be robust.

The patient-specific data were imported into a finite element method programme (ADINA) for FSI analysis. The fluid and solid domain solutions for patients A and B were coupled using the arbitrary Lagrangian–Eulerian algorithm. For patient C, no velocity information was available, therefore only static analysis was performed, using a pressure corresponding to the peak systolic pressure from Fig. 4. In order to assess the influence of FSI on stress patterns within the aneurysm wall, solid models containing the thrombus and the wall for patients A and B were created. For these models, decoupled static structural analyses were performed at the peak systolic pressure. Results were compared with those of FSI simulations and changes in stress pattern due to the contribution of pulsatile flow inside the aneurysm were quantified.

Using the same methodology, the lumen and wall models of a normal descending aorta were created (details of the image sets used for this purpose are given in Table 1). Since the healthy volunteer presented no ILT in his aorta, the wall boundary for each transverse slice was created using a constant thickness dilation of the corresponding lumen boundary. The inlet velocity waveform was taken from the literature (Olufsen et al., 2000) since MR velocity mapping was not performed on this subject. The outlet pressure was the same as for patients A and B, and both FSI and static stress analyses were carried out for the normal aorta.

Grid independence test was performed for each individual case concerned. The number of subdivisions in the fluid and wall domain was increased until differences in velocity (for the fluid domain) and maximum wall stress (for the wall domain) were less than 5%. The number of nodes used for patient A was 27 030 for the wall and 51 579 for the lumen; the number of nodes for patient B was 36 160 for the wall and 25 008 for the lumen; while 25 252 nodes were used for the wall model of patient C. For the normal aorta, 20 520 nodes were used for the wall and 20 808 nodes for the lumen.

3. Results

Three models of TA and a normal descending aorta with patient-specific geometry were analysed using ADINA 8.2 (ADINA R&H Inc.): for patients A and B and for the control case fully coupled FSI simulations were performed, as well as static analysis using the maximum systolic pressure; for patient C, only decoupled static structural analysis was performed. The simulations were carried out for three cardiac cycles, but the results of both stress and flow patterns were found to be periodic after the second cardiac cycle.

Fig. 5 shows the stress patterns on the outer wall of all cases using results from the decoupled solid stress analysis models. It is interesting to note that stress levels in all TA models are higher than those in the normal aorta which has a fairly uniform stress distribution. Although all patients had maximum diameters close to the threshold for surgical intervention (surgery is usually recommended for aneurysms of 6.5 cm in the descending aorta) (Elefteriades, 2002), the maximum stress in patient A is higher than those for patients B and C as summarized in Table 2. High wall stress is concentrated at one location in patient A, but appears at more than one spot in patients B and C. This is due to the different shape of the aneurysms, as well as the amount and distribution of thrombus in them. Fig. 6 shows stress distributions in longitudinal sections of the aneurysms as well as transverse sections at locations where high stresses occur (as indicated by the dashed lines on the longitudinal sections). Areas of high stress are highlighted by circles, which are mostly located on the opposite side to the thrombus. Apparently, the sections where thrombus is concentrated on one side experience increased stress on the other side of the wall, whereas stress is more uniformly distributed in sections where thrombus is absent or evenly distributed along the circumference. It can also be observed that areas shrouded by thrombus present very low levels of stress showing how ILT protects the wall locally from the blood pressure (Di Martino and Vorp, 2003).

Since FSI simulations were performed for patients A and B as well as the normal aorta, flow patterns and WSS were obtained for these cases. In Fig. 7, WSS patterns at peak systole are presented: for both patients the area of low WSS coincides with the location of the thrombus (indicated by the longitudinal section of the wall model on the left). By comparing patients A and B, it can be noted that for patient B low shear stress is present over the entire lumen/wall boundary, while for patient A the low WSS area is concentrated around the aneurysm bulge. WSS in the normal aorta is relatively uniform with small spatial variation. Detailed flow patterns inside the aneurysms are shown in Fig. 8 to examine the link between abnormal flow patterns and the presence of thrombus. For both patients A and B, flow recirculation is observed in the aneurysm bulge, located in the middle of the descending thoracic aorta of patient A and in two regions for patient B (as shown in the horizontal sections of Fig. 8). As shown by Bluestein et al. (1996) for AAA models, platelets trapped in recirculating zones tend to be deposited in areas of low shear stress, since this and the

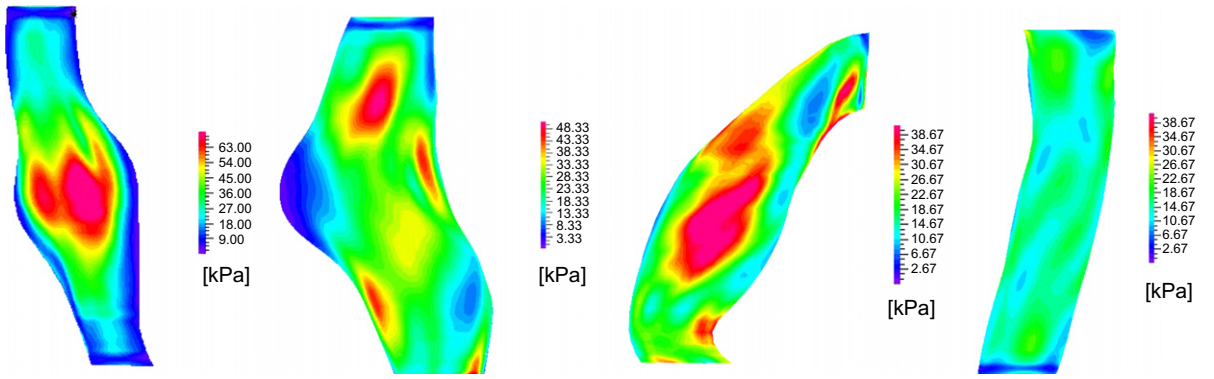

Fig. 5. Stress patterns on the outer wall for patients A, B and C and the normal aorta (units: kPa); high wall stress is concentrated at one location in patient A, but appears at more than one spot in patients B and C; the stress distribution for the normal aorta is fairly uniform.

Table 2
Summary of the maximum diameter and peak wall stress in all cases examined (the results are for the static stress analysis)

	Patient A	Patient B	Patient C	Control case
D_{max} (cm)	7	6.2	7.0	2.5
σ_{max} (kPa)	79.36	51.81	48.61	41.54

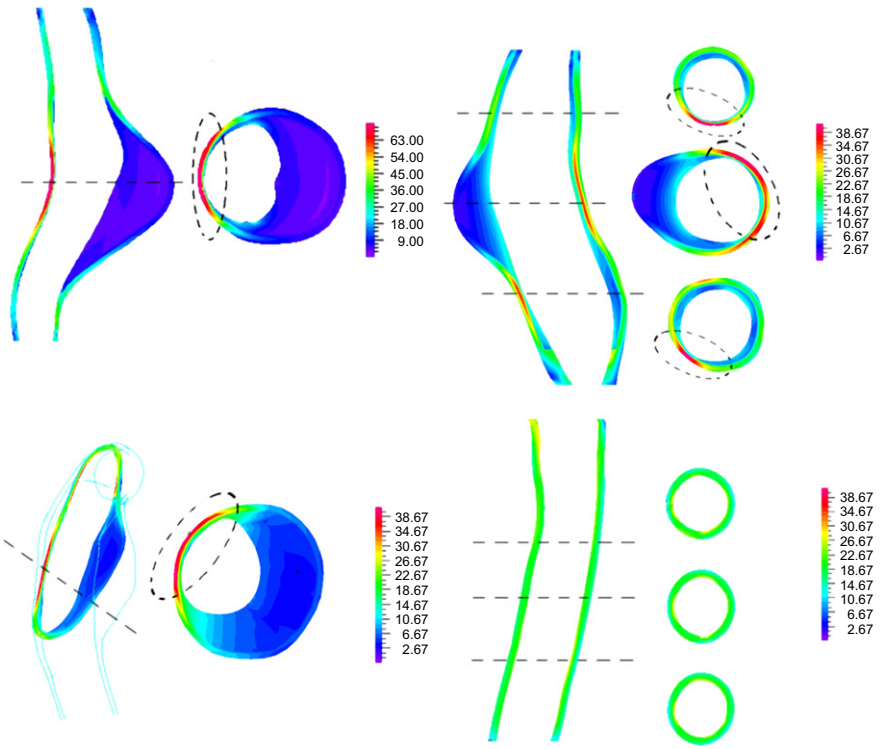

Fig. 6. Stress patterns in a longitudinal section (oblique-longitudinal for patient C) and transverse sections at locations where high wall stresses occur. The dashed lines indicate the level of the transverse locations; areas of high stress are highlighted by circles (units: kPa).

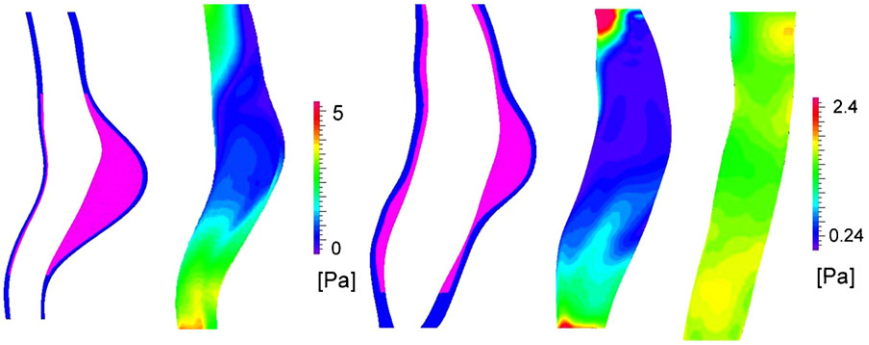

Fig. 7. Wall shear stress at peak systole for patients A and B as well as the normal aorta (units: Pa). Longitudinal sections of the wall domains for the two TA models are also shown to demonstrate the correspondence between low WSS regions and locations of thrombus.

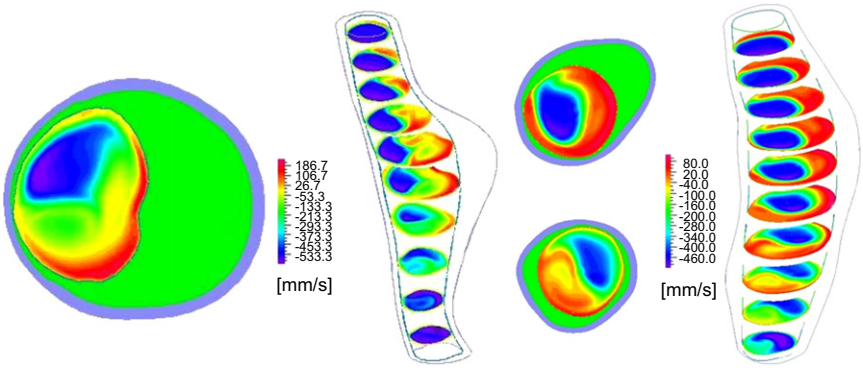

Fig. 8. Flow patterns inside the TA models for patients A and B and the normal aorta. Note that forward flow points downwards and has a negative value in the adopted coordinate system. In each case, the flow pattern at the middle section of the aneurysm bulge is given on the left (forward flow is shown in blue), the thrombus layer is coloured in green while the wall is in violet. Reverse flow (in red) occurs on the thrombus side; (units: mm/s).

Table 3
Comparison of the maximum stress level as calculated using fully coupled FSI and static solid simulations

	Patient A			Patient B			Control case		
	FSI	Structure only	Δ (%)	FSI	Structure only	Δ (%)	FSI	Structure only	Δ (%)
σ_{max} (kPa)	82.15	79.36	3.4	51.92	51.81	0.1	41.80	41.54	0.6

presence of vortices cause prolonged contact of the platelets with the surface in the layer of slow fluid motion (Bluestein et al., 2000). This can provide an insight into the mechanism that promotes the thrombus renewal and possibly enlargement inside the aneurysm.

Finally, results from the FSI simulations were compared with those of the static structural models, where wall stress was calculated without accounting for the pulsatile flow inside the aneurysms. As summarized in Table 3, differences in predicted maximum wall stress are very small and can be neglected.

4. Discussion

TA is a pathology involving the enlargement of the aorta in the inferior thoracic area. The mortality for this pathology is high (15% for ruptured aneurysms) and post-operative complications occur in 4.6% of the patients. In this

study three aneurysms with similar features, all located in the thoracic aorta just above the diaphragm, were compared. ILT was present in all patients in the region of the aneurismal bulge with asymmetric thrombus distribution. FSI simulations as well as static structural analyses were performed using patient-specific geometry and flow conditions, together with pulsatile pressure waves and material properties extracted from the literature.

The results show that peak wall stress is located in the aneurysm bulge for all patients examined, on the side of the wall which is free from thrombus (Fig. 6). Based on findings reported in the literature, the presence of ILT in AAAs is thought to have a protective effect on the aortic wall (Wang et al., 2002; Mower et al., 1997; Schurink et al., 2000). Our results show that the distribution of ILT in the aneurysm bulge is nonuniform, resulting in reduced stress in the region of the wall covered by ILT but significantly increased wall stress in the region 'unprotected' by ILT. The shape of ILT as well as its thickness distribution are important in determining stress pattern in aneurysm walls; a circumferentially uniformly distributed ILT will reduce the average and peak stress levels, whereas a non-uniform ILT will put part of the wall at risk of higher wall stress. Similar results were found previously using simplified aneurysm models (Di Martino et al., 1998). The stress levels presented here are generally lower than those reported in other studies where similar boundary conditions were applied (Di Martino et al., 2001; Wolters et al., 2005); however, these studies were on AAAs, which are characterized by different material properties (Raghavan and Vorp, 2000); therefore, the stress levels are not directly comparable.

It should be noted that the actual effect of ILT may depend on the thrombus composition (which in this work has been assumed to be a homogeneous material) and material properties; for this study values from the literature were used, which correspond to population-mean values (Vorp et al., 2003; Raghavan and Vorp, 2000). Due to the absence of symmetry in patient-specific models, it was not possible to implement a biaxial constitutive relationship for the aneurysm wall, neither was it possible to divide the thrombus into luminal and medial layers due to the lack of MR tissue contrast between the two. However, previous uniaxial tensile testing and recent biaxial study have shown that there is no significant difference in stiffness between the longitudinal and circumferential directions in ILT (Wang et al., 2001), suggesting that it may be reasonable to treat ILT as an isotropic material. Furthermore, Di Martino and Vorp (2003) have demonstrated in an AAA model that differentiating the material properties of the thrombus layers does not significantly change the computed stress levels. With regard to material properties of the aneurismal aorta, several studies have found that both TA and AAA tissues exhibit anisotropic behaviour (Fukui et al., 2005). Using thoracic aortic tissue, Fuikui et al. showed that the aneurysm became more anisotropic with the increase in stiffness, and the wall was stiffer circumferentially than longitudinally in specimens where the exact direction of the fibres was clearly visible, as was also found in the previous uniaxial study on AAA by Thubrikar et al. (2001). Vande Geest et al. (2006a, b) derived a possible equation for the biaxial mechanical response of AAAs: the comparison of the uniaxial response for AAA tissue with the biaxial curve showed a stiffer behaviour in case of isotropic material for low-strain regions. The use of isotropic material properties is a strong limitation for the present work; however, the application of the anisotropic properties is not feasible when the exact direction of the fibres is not available. The effect of anisotropic material properties was evaluated using AAA models and summarized by Vorp (2007). It was found that models using anisotropic material properties predicted larger areas of high wall stress and higher peak stresses than those assuming an isotropic material property, but no qualitative change was noted in stress distribution pattern.

By comparing the maximum wall stresses among all cases, it is clear that the magnitude of peak wall stress is not directly proportional to the maximum aneurysm diameter. Patients A and C have the same maximum aneurysm diameter, but the peak stress of patient A is 63% higher than that of patient C. Patient B has a smaller aneurysm but marginally higher peak wall stress than that of patient C, whose peak wall stress is about 17% higher than the control case. If peak wall stress were used as a surgical criterion instead of the maximum aneurysm diameter, patient C would be regarded as having lower risk of rupture than patient A. However, a comprehensive biomechanics-based assessment of rupture potential of aortic aneurysms should also include evaluation of wall strength, which may be affected by age, family history, smoking history, as well as the aneurysm growth rate and the presence of ILT (Vande Geest et al., 2006a, b).

The WSS patterns show that low shear stress is present in the bulge area, and patient B has a larger area of low WSS. This coincides with the location and distribution of thrombus in this patient, implying the role of low WSS in the formation and propagation of ILT. It has been reported that platelet activation is correlated with low WSS (Savage et al., 1996) and its deposition is enhanced by flow recirculation (Bluestein et al., 1996) and low WSS (Bluestein et al., 2000), that allow prolonged contact of the platelets with the lumen surface. It has also been found that interaction between the fibrinogen and platelet receptors occurs at low shear stress levels and the luminal layer of ILT is itself highly thrombogenic (Touat et al., 2006). Our results not only provide further evidence that regions of low WSS co-localize with areas where ILT is formed, but also imply that these areas may be susceptible to further thrombus renewal and propagation. A sequential study of the aneurysm from its early stage of development would help to shed light on the potential relationship between thrombus formation and the initial flow patterns, but unfortunately follow-up data for the patients reported here are not available. A similar correspondence between low WSS and location of thrombus was found by Leung et al. (2006) in patient-specific AAA models.

Comparisons between results from the FSI simulations and static stress analyses show that the difference in predicted peak wall stress is very small, being 3.4% for patient A, 0.1% for patient B and 0.6% for the normal aorta. Furthermore, the location of peak wall stress remains the same between the FSI and static solid models. This agrees with other findings in the literature (Leung et al., 2006), where it is pointed out that the difference between stress levels in the fully coupled models and static models is due to the flow-induced pressure, which is negligible compared to the pulse pressure load. In the present work, the stress variation is higher than that found by Leung et al. but lower than that reported by Scotti et al. (2005) and Papaharilaou et al. (2006). In the first study, a higher internal pressure was used (120 mmHg versus 40 mmHg of the present study), hence the sensitivity of the computed stress to the pressure drop along the vessel is lower than in the present study. In Scotti's work, a 1.5 mm wall was used to model a hypothetical abdominal aneurysm, as opposed to the wall thickness of approximately 3 mm measured from *in vivo* images of the patients in this study: a thinner wall is more sensitive to the internal pressure variation; therefore, a larger difference between FSI and static analysis results can be expected. The same applies to Papaharilou et al.'s work which was based on a decoupled fluid and structure approach, so that the flow pattern and pressure drop calculated from the fluid model were not influenced by the wall motion since the wall was kept rigid. In all these studies, as well as in the present, the wall stress in the static analysis is underestimated in comparison with that obtained from the fully coupled solution.

In the present study, the aortic wall thickness (excluding the ILT thickness) was assumed constant throughout the aneurysm due to insufficient spatial resolution of the MRI protocol adopted for *in vivo* scans. Although this is a common assumption adopted by other researchers (Venkatasubramaniam et al., 2004; Di Martino et al., 2001; Leung et al., 2006; Papaharilaou et al., 2006; Wang et al., 2002), it represents a major limitation since wall thickness has been recognized as an important factor in determining the peak wall stress in aneurysm models (Venkatasubramaniam et al., 2004; Scotti et al., 2005). In order to customize the creation of the wall model for each patient, a number of wall thickness measurements were made from the MR images at locations where the boundary between the aortic wall, ILT and lumen was clearly visible. However, due to the lack of contrast between the wall and ILT layers in many regions and due to the ambiguity in some images caused by respiration, a faithful reconstruction of the wall thickness for the entire TA was impossible. Nevertheless, the present work has moved a step further by employing an average constant wall thickness estimated for each individual patient together with realistic ILT thickness reconstructed from *in vivo* images. Since the total thickness consisting of the wall and the ILT layer was faithfully reconstructed, the assumption of a constant thickness for the wall layer is unlikely to have a significant effect on the predicted wall stress. Future improvement in MRI spatial resolution and tissue contrast may allow true wall thickness to be derived from *in vivo* images for patient-specific simulations.

5. Conclusion

To conclude, in this work the stress pattern and flow conditions of three patients with TA have been analysed, using finite element simulation with patient-specific geometry. The presence of ILT has been shown to affect the stress distribution in the aneurysm and partially protect the aortic wall from the blood pressure (Mower et al., 1997); however, asymmetric ILT tends to cause part of the wall (uncovered by ILT) to be exposed to high wall stress. Results from the patient-specific TA models were compared with those of a normal aorta and it has been found that the normal aorta has a much more uniformly distributed wall stress and WSS. Maximum wall stresses in all TA models are higher than in the normal aorta, and values of maximum wall stress are not directly related to the maximum aneurysm diameter, providing further evidence that patient-specific wall stress analysis is necessary for a more reliable assessment of the rupture risk of aortic aneurysms. Comparisons between the fully coupled FSI simulations and solid models demonstrate that FSI simulations are not necessary for wall stress prediction. It is hoped that the present analysis will be extended to a large group of patients, in order to provide further information on the role of anatomical features such as the shape and wall composition on the stress pattern and consequently the potential rupture of thoracic aneurysms.

Aknowledgement

This project was supported by the British Heart Foundation (FS/03/119).

References

Augst, A.D., Barratt, D.C., Hughes, A.D., Glor, F.P., Mc, G.T.S.A., Xu, X.Y., 2003. Accuracy and reproducibility of CFD predicted wall shear stress using 3-D ultrasound images. ASME Journal of Biomechanical Engineering 125 (2), 218–222.

Bluestein, D., Niu, L., Schoephoerster, R.T., Dewanjee, M.K., 1996. Steady flow in an aneurysm model: correlation between fluid dynamics and blood platelet deposition. ASME Journal of Biomechanical Engineering 118 (3), 280–286.

Bluestein, D., Rambod, E., Gharib, M., 2000. Vortex shedding as a mechanism for free emboli formation in mechanical heart valves. ASME Journal of Biomechanical Engineering 122 (2), 125–134.

Cheong, P.L., 2004. Magnetic resonance imaging and computater simulation of haemodynamics at the human aortic bifurcation. Ph.D. Thesis, Imperial College London.

Crawford, E.S., Crawford, J.L., Safi, H.J., Coselli, J.S., Hess, K.R., Brooks, B., Norton, H.J., Glaeser, D.H., 1986. Thoracoabdominal aortic aneurysms: preoperative and intraoperative factors determining immediate and long-term results of operations in 605 patients. Journal of Vascular Surgery 3 (3), 389–404.

Culliford, A.T., Ayvaliotis, B., Shemin, R., Colvin, S.B., Isom, O.W., Spencer, F.C., 1983. Aneurysms of the descending aorta. Surgical experience in 48 patients. The Journal of Thoracic and Cardiovascular Surgery 85 (1), 98–104.

Di Martino, E.S., Vorp, D.A., 2003. Effect of variation in intraluminal thrombus constitutive properties on abdominal aortic aneurysm wall stress. Annals of Biomedical Engineering 31 (7), 804–809.

Di Martino, E., Mantero, S., Inzoli, F., Melissano, G., Astore, D., Chiesa, R., Fumero, R., 1998. Biomechanics of abdominal aortic aneurysm in the presence of endoluminal thrombus: experimental characterisation and structural static computational analysis. European Journal of Vascular and Endovascular Surgery 15 (4), 290–299.

Di Martino, E.S., Guadagni, G., Fumero, A., Ballerini, G., Spirito, R., Biglioli, P., Redaelli, A., 2001. Fluid-structure interaction within realistic three-dimensional models of the aneurysmatic aorta as a guidance to assess the risk of rupture of the aneurysm. Medical Engineering and Physics 23 (9), 647–655.

Elefteriades, J.A., 2002. Natural history of thoracic aortic aneurysms: indications for surgery, and surgical versus nonsurgical risks. The Annals of Thoracic Surgery 74 (5), S1877–S1880 discussion S1892-1878.

Fillinger, M.F., Marra, S.P., Raghavan, M.L., Kennedy, F.E., 2003. Prediction of rupture risk in abdominal aortic aneurysm during observation: wall stress versus diameter. Journal of Vascular Surgery 37 (4), 724–732.

Fukui, T., Matsumoto, T., Tanaka, T., Ohashi, T., Kumagai, K., Akimoto, H., Tabayashi, K., Sato, M., 2005. *In vivo* mechanical properties of thoracic aortic aneurysmal wall estimated from *in vitro* biaxial tensile test. Bio-medical Materials and Engineering 15 (4), 295–305.

LeMaire, S.A., Miller III, C.C., Conklin, L.D., Schmittling, Z.C., Coselli, J.S., 2003. Estimating group mortality and paraplegia rates after thoracoabdominal aortic aneurysm repair. The Annals of Thoracic Surgery 5 (2), 508–513.

Leung, J.H., Wright, A.R., Cheshire, N., Crane, J., Thom, S.A., Hughes, A.D., Xu, Y., 2006. Fluid structure interaction of patient specific abdominial aortic aneurysms: a comparison with solid stress models. Biomedical Engineering Online 5 (1), 33.

Long, Q., Xu, X.Y., Ariff, B., Thom, S.A., Hughes, A.D., Stanton, A.V., 2000. Reconstruction of blood flow patterns in a human carotid bifurcation: a combined CFD and MRI study. Journal of Magnetic Resonance Imaging 11 (3), 299–311.

Machida, K., Tasaka, A., 1980. CT patterns of mural thrombus in aortic aneurysms. Journal of Computer Assisted Tomography 4 (6), 840–842.

Moore, J.A., Steinman, D.A., Holdsworth, D.W., Ethier, C.R., 1999. Accuracy of computational hemodynamics in complex arterial geometries reconstructed from magnetic resonance imaging. Annals of Biomedical Engineering 27 (1), 32–41.

Mower, W., Quinones, W., Gambhir, S., 1997. Effect of intraluminal thrombus on abdominal aortic aneurysm wall stress. Journal of Vascular Surgery 26 (4), 602–608.

Olufsen, M.S., Peskin, C.S., Kim, W.Y., Pedersen, E.M., Nadim, A., Larsen, J., 2000. Numerical simulation and experimental validation of blood flow in arteries with structured-tree outflow conditions. Annals of Biomedical Engineering 28 (11), 1281–1299.

Papaharilaou, Y., Ekaterinaris, J.A., Manousaki, E., Katsamouris, A.N., 2006. A decoupled fluid structure approach for estimating wall stress in abdominal aortic aneurysms. Journal of Biomechanics 40 (2), 367–377.

Raghavan, M.L., Vorp, D.A., 2000. Toward a biomechanical tool to evaluate rupture potential of abdominal aortic aneurysm: identification of a finite strain constitutive model and evaluation of its applicability. Journal of Biomechanics 33 (4), 475–482.

Savage, B., Saldivar, E., Ruggeri, Z.M., 1996. Initiation of platelet adhesion by arrest onto fibrinogen or translocation on von Willebrand factor. Cell 84 (2), 289–297.

Schurink, G., van Baalen, J., Visser, M., van Bockel, J., 2000. Thrombus within an aortic aneurysm does not reduce pressure on the aneurysmal wall. Journal of Vascular Surgery 31 (3), 501–506.

Scotti, C.M., Shkolnik, A.D., Muluk, S.C., Finol, E.A., 2005. Fluid-structure interaction in abdominal aortic aneurysms: effects of asymmetry and wall thickness. Biomedical Engineering Online 4 (4), 64.

Thubrikar, M.J., Labrosse, M., Robicsek, F., Al-Soudi, J., Fowler, B., 2001. Mechanical properties of abdominal aortic aneurysm wall. Journal of Medical Engineering and Technology 25 (4), 133–142.

Touat, Z., Ollivier, V., Dai, J., Huisse, M.G., Bezeaud, A., Sebbag, U., Palombi, T., Rossignol, P., Meilhac, O., Guillin, M.C., Michel, J.B., 2006. Renewal of mural thrombus releases plasma markers and is involved in aortic abdominal aneurysm evolution. The American Journal of Pathology 168 (3), 1022–1030.

Vande Geest, J.P., Sacks, M.S., Vorp, D.A., 2006a. The effects of aneurysm on the biaxial mechanical behavior of human abdominal aorta. Journal of Biomechanics 39 (7), 1324–1334.

Vande Geest, J.P., Di Martino, E.S., Bohra, A., Makaroun, M.S., Vorp, D.A., 2006b. A biomechanics-based rupture potential index for abdominal aortic aneurysm risk assessment: demonstrative application. Annals of the New York Academy of Sciences 1085, 11–21.

Venkatasubramaniam, A.K., Fagan, M.J., Mehta, T., Mylankal, K.J., Ray, B., Kuhan, G., Chetter, I.C., McCollum, P.T., 2004. A comparative study of aortic wall stress using finite element analysis for ruptured and non-ruptured abdominal aortic aneurysms. European Journal of Vascular and Endovascular Surgery 28 (2), 168–176.

Vorp, D.A., 2007. Biomechanics of abdominal aortic aneurysm. Journal of Biomechanics 40 (9), 1887–1902.

Vorp, D.A., Schiro, B.J., Ehrlich, M.P., Juvonen, T.S., Ergin, M.A., Griffith, B.P., 2003. Effect of aneurysm on the tensile strength and biomechanical behavior of the ascending thoracic aorta. The Annals of Thoracic Surgery 75 (4), 1210–1214.

Wang, D.H., Makaroun, M., Webster, M.W., Vorp, D.A., 2001. Mechanical properties and microstructure of intraluminal thrombus from abdominal aortic aneurysm. ASME Journal of Biomechanical Engineering 123 (6), 536–539.

Wang, D.H., Makaroun, M.S., Webster, M.W., Vorp, D.A., 2002. Effect of intraluminal thrombus on wall stress in patient-specific models of abdominal aortic aneurysm. ASME Journal of Vascular Surgery 36 (3), 598–604.

Webb, T.H., Williams, G.M., 1999. Thoracoabdominal aneurysm repair. Cardiovascular Surgery 7 (6), 573–585.

Wolters, B.J., Rutten, M.C., Schurink, G.W., Kose, U., de Hart, J., van de Vosse, F.N., 2005. A patient-specific computational model of fluid-structure interaction in abdominal aortic aneurysms. Medical Engineering and Physics 27 (10), 871–883.

Wood, N.B., Weston, S.J., Gosman, A.D., 2001. Combined MR imaging and CFD simulation of flow in the human descending aorta. Journal of Magnetic Resonance Imaging 13, 699–713.